Water Resources Research

RESEARCH ARTICLE
10.1029/2022WR032385

Stable Water Isotopologue Fractionation During Soil-Water Evaporation: Analysis Using a Coupled Soil-Atmosphere Model

Stefanie Kiemle[1], Katharina Heck[1], Edward Coltman[1], and Rainer Helmig[1]

[1]Institute for Modelling Hydraulic and Environmental Systems, Department of Hydromechanics and Modelling of Hydrosystems, University of Stuttgart, Stuttgart, Germany

Key Points:

- Modeling stable water isotopologue fractionation in the unsaturated zone during evaporation from bare soils
- Using coupled soil-atmosphere models deriving kinetic isotopic effects

Correspondence to:

S. Kiemle,
stefanie.kiemle@iws.uni-stuttgart.de

Citation:

Kiemle, S., Heck, K., Coltman, E., & Helmig, R. (2023). Stable water isotopologue fractionation during soil-water evaporation: Analysis using a coupled soil-atmosphere model. *Water Resources Research*, *59*, e2022WR032385. https://doi.org/10.1029/2022WR032385

Received 16 MAR 2022
Accepted 20 JAN 2023

Abstract The atmosphere-soil system forms a highly coupled system, which makes key processes such as evaporation complex to analyze as the mass, energy, and momentum transfer is influenced by both domains. To enhance the understanding of evaporation processes from soils, stable water isotopologues are suitable tools to trace water movement within these systems as heavier isotopologues enrich in the residual liquid phase. Due to the complex coupled processes involved in simulating soil-water evaporation accurately, quantifying fractionation during flow and transport processes at the soil-atmosphere interface remains an open research area. In this work, we present a multi-phase multi-component transport model that resolves flow through the near-surface atmosphere and the soil, and models transport and fractionation of the stable water isotopologues using the numerical simulation environment DuMu^x. Using this coupled model, we simulate transport and fractionation processes of stable water isotopologues in soils and the atmosphere by solving compositional flow equations and by using suitable coupling conditions at the soil-atmosphere interface instead of commonly used parameterization. In a series of examples of evaporation from bare soil, the transport and distribution of stable water isotopologues are evaluated numerically with varied conditions and assumptions, including different atmospheric conditions (turbulent/laminar flow, wind speed) and their impact on the spatial and temporal distribution of the isotopic composition. Building on these results, we observed how the enrichment of the isotopologues in soil is linked with the different stages of the evaporation process. A qualitative study is conducted to verify single fractionation processes in our approach.

1. Introduction

Stable water isotopologues are commonly used as natural tracers to determine the water movement within the unsaturated zone (e.g., Sprenger et al., 2016, 2018). Analyzing their compositions in water has proven to be a suitable tool for better understanding evaporation at the soil-atmosphere interface and mixing processes within soils. For instance, the location of the evaporation front within the soil can be identified by measuring the isotopic composition (Rothfuss et al., 2015). During evaporation, stable water isotopologues are affected by fractionation processes. This process can be divided into equilibrium and kinetic fractionation (Craig, 1961; Craig & Gordon, 1965). Due to their differences in vapor pressure (equilibrium fractionation) and their varied diffusion coefficients (kinetic fractionation), the transport and flow behavior of heavier stable water isotopologues (e.g., ${}^2H^1HO$ and $H_2^{18}O$) is different in comparison to the lighter isotopologue $H_2^{16}O$. In the following, we will denote $H_2^{16}O$ as ordinary water, as it is the most common isotopologue.

Whereas the description of the equilibrium fractionation is consistent in literature (Horita & Wesolowski, 1994; Luz et al., 2009; Majoube, 1971), in terms of the kinetic fractionation, there are uncertainties in defining the relationship between the vapor diffusion coefficients under evaporating conditions (e.g., Luz et al., 2009; Quade et al., 2018). The major challenge in determining the kinetic fractionation correctly is how to include the influence of atmospheric properties like wind velocities, temperature, and humidity, but also soil-specific properties such as surface roughness and capillarity (Quade et al., 2018).

In the past, many one-dimensional process-based models have been developed: ODWISH (Shurbaji & Phillips, 1995), MOISE (Mathieu & Bariac, 1996; Melayah et al., 1996), SiSPAT-Isotope (Braud et al., 2005), Soil-Litter-Iso (Haverd & Cuntz, 2010), SWIS (Müller et al., 2014; Sprenger et al., 2018), HYDRUS-1D (Zhou et al., 2021). With these 1D model approaches, fractionation processes within the unsaturated zone and in the interface region can be simulated. However, these models only cover the influence of the atmosphere by including

evaporation boundary conditions and using parameterizations to describe the kinetic fractionation. Thus, the influence of the free-flow with varying wind conditions, humidities, and temperatures on the fractionation process can only be modeled for certain conditions (i.e., some factors are only valid or tested for a certain range of wind velocities) where suitable parameterizations are available. Additionally, the spatial distribution of the isotopologues is analyzed in 1D, and possible multidimensional effects cannot be analyzed with these models.

Concerning isotopologue transport models on a catchment model scale, some models can be found in literature: TAC^{D} (Uhlenbrook et al., 2004), NASA-Giss ModelIE (Aleinov & Schmidt, 2006), CMF (Kraft et al., 2011; Windhorst et al., 2014), ECHAM5-JSBACH-wiso (Haese et al., 2012), ORCHIDEE (Risi et al., 2016), iCLM4 (Wong et al., 2017), EcoH2O-iso* (Kuppel et al., 2018), TOUGH2 (Jiang et al., 2018). However, besides the issue that these models operate on a larger scale with lower resolution (land surface or catchment models) than our interest, which is to analyze isotopologue transport at an intermediate scale, suitable for analyzing laboratory experiments on a REV scale, they also rely on parameterizations to describe the isotope transport and fractionation. Depending on scale and application, using parameterizations, especially in land surface or catchment models, can be of course very suitable in many cases. However, for a detailed process analysis, the presented approach can give more insights.

With our approach, we also want to include the influence of atmospheric flow on the isotopic fractionation processes in the porous-medium domain with thermodynamic consistency by accounting for the flow and transport in the free-flow domain and coupling the free-flow to the porous-medium domain. By resolving and coupling both domains we can derive the kinetic fractionation process for the interface region without relying on any fractionation parameterizations. To our knowledge, there is no stable water isotopologue transport model, which resolves both domains and couples the free-flow and the porous-medium domain on the REV scale.

In the following, we present a multi-dimensional stable water isotopologue transport model which couples a free-flow domain representing the atmosphere and a porous-medium domain and ensures mass, momentum, and energy conservation. Evaporation of both ordinary water and the heavier isotopologues can be described under varying free-flow conditions, for example, varying wind speeds including turbulent and laminar flow conditions. This means we can describe the fractionation process in the free-flow domain, the interface region, and the porous-medium domain without implementing the commonly used fractionation parameterizations. This allows us to analyze the flow and transport of the isotopologues together with the evaporation process of ordinary water. Further, the influence of the different stages of the evaporation processes on isotopologue behavior can be reviewed. It also allows us to isolate physical factors, analyzing the processes contributing to isotopologue fractionation independently.

2. Methods

In this section, we describe the principles of fractionation processes of stable water isotopologues during evaporation from soils (Section 2.1), as well as the applied coupled model concept (Section 2.2). This model concept includes the description of mass and energy transfer within the porous-medium domain Ω_{pm}, within the atmospheric free-flow domain Ω_{ff}, and the coupling concept connecting the domains. At the end of the chapter, the numerical model is briefly explained in Section 2.3.

2.1. Fractionation Processes of Stable Water Isotopologues

Craig and Gordon (1965) proposed a model for isotopic effects during evaporation from a free water surface. The so-called Craig-Gordon model describes the effects of the different transport mechanisms and fractionation processes between the water surface and the ambient air. The original Craig-Gordon model is distributed into three zones. These zones can be adapted for the application in porous medium by extending the zones to the soil-water evaporation front. These zones are as follows: (a) a turbulent zone where turbulent mixing occurs and the isotopic composition becomes constant; (b) a diffusive zone defined by the viscous sub-layer where diffusive transport dominates and kinetic fractionation is the leading fractionation process; and (c) an interface zone where the liquid and vapor phase are in isotopic equilibrium inside the porous medium and equilibrium fractionation governs the fractionation process. In Figure 1, the isotopic composition profile and the classification into the specific fractionation zone are illustrated.

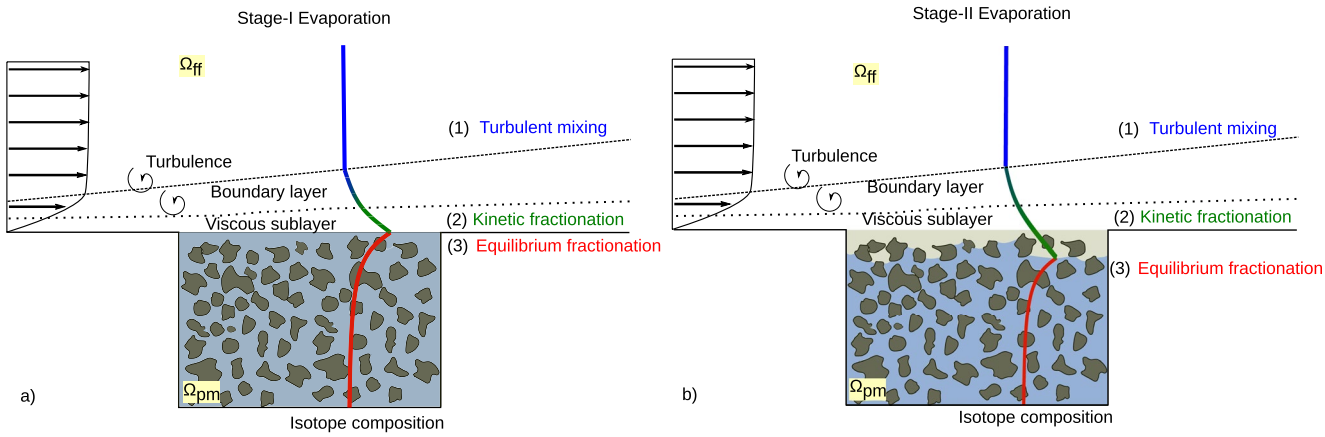

Figure 1. Isotopic composition profiles during (a) stage-I evaporation, (b) stage-II evaporation and the classification into their respective isotopic fractionation processes.

Analyzing the enrichment of isotopic species in soils can be used to determine the depth or progression of the evaporation front in unsaturated soils. The evaporation front can be located at the maximal gradient of the isotopic composition (Rothfuss et al., 2015). This and the impact of the different evaporation stages on the enrichment process are depicted in Figure 1.

During stage-I evaporation (Figure 1a), the atmospheric evaporation potential is satisfied at the soil-atmosphere interface by capillary recharge. As the soil dries out further, the evaporation rate reduces as stage-II evaporation begins (Figure 1b; e.g., Lehmann et al., 2008). Here, liquid water at the interface is less mobile as residual saturation is approached and evaporation is possible through diffusive transport. While the soil dries out, the position of the isotopic zones rearranges. The interface zone, characterized by equilibrium fractionation, moves with the evaporation front downwards, and the diffusive zone, characterized by kinetic fractionation, is thereby extended. The maximal gradient of the isotopic composition and so the evaporation front is no longer located at the porous-medium domain surface, but below the soil surface, in the transition between the diffusive and interface zone.

In most models describing isotopic fractionation, the main driving processes for isotopic fractionation in soils and at the soil-atmosphere interface are commonly expressed by the equilibrium fractionation factor and the kinetic fractionation factor. In general, the fractionation factor describes the tendency of two components κ to separate from their mixture. For the kinetic fractionation factor, which describes the fractionation of isotopic species caused by the difference in diffusive transport of water and its isotopologues, many approaches exist. Barnes and Allison (1984) described the kinetic fractionation factor considering only molecular transport. Dongmann et al. (1974) extended the definition of Barnes and Allison (1984) by involving free-flow properties. Besides these definitions, Brutsaert (1975), Craig and Gordon (1965), Gat (1971), Mathieu and Bariac (1996), Quade et al. (2018) published alternative formulations. As stated before, in our transport model, we do not rely on the kinetic fractionation factor. As we describe the transport of each isotopologue with different diffusion coefficients and resolve the atmosphere (as a free-flow domain) possible kinetic effects, for example, due to turbulent flow, are inherently included in the description of the transport. In Section 3, details about the diffusion coefficients used can be found.

The equilibrium fractionation factor (in the following denoted by β^i_{eq}) is defined by the different vapor pressures of the heavier isotopologues p^i_g and the vapor pressure of the lighter ordinary water $p_g^{H_2^{16}O}$ and is commonly expressed by the dependence on the temperature T and coefficients that can be chosen from the literature. In our model, the fractionation factor is used to describe the difference in vapor pressure of the different isotopologues.

$$p^i_g = \beta^i_{eq} p_g^{H_2^{16}O} = \exp\left(-\left(\frac{A}{T^2} + \frac{B}{T} + C\right)\right) p_g^{H_2^{16}O}. \quad (1)$$

As we assume chemical equilibrium, we compute the phase compositions based on Henry's and Raoult's law. The equilibrium fractionation factor is smaller than 1, which leads to the enrichment of the isotopologues in liquid water compared to ordinary water. More information about the used coefficients can be found in the appendix.

To summarize, in the presented coupled transport model, equilibrium and kinetic fractionation effects can be derived from solving two-phase four-component transport equations in the porous medium and one-phase four-component transport equations in the free-flow domain. Both domains (the free-flow domain describing the atmosphere and the porous-medium domain) are coupled with the help of suitable coupling conditions that ensure mass, momentum, and energy conservation.

In the following, model concepts for the porous-medium domain, the free-flow domain, and the coupling conditions are presented.

2.2. Coupled Model Concepts

2.2.1. Porous-Medium Domain

The porous-medium flow domain is described by a multiphase Darcy's law in combination with a mass and energy balance to describe non-isothermal, multiphase flow. The mass balance equation for the component transport is written as the following:

$$\sum_{\alpha\in\{\mathrm{l,g}\}}\left(\phi\frac{\partial(\rho_\alpha S_\alpha X_\alpha^\kappa)}{\partial t}+\nabla\cdot\mathbf{v}_\alpha\rho_\alpha X_\alpha^\kappa+\sum_\kappa\nabla\cdot\left(\mathbf{D}_{pm,\alpha}^\kappa\rho_\alpha\nabla X_\alpha^\kappa\right)\right)=0, \tag{2}$$

Here $\mathbf{D}_{pm,\alpha}^\kappa$ denotes the effective binary diffusion coefficient in the porous medium. Phase saturations are denoted by S_α and ρ_α is the density of the phase. X_α^κ is the mass fraction that is defined by $X_\alpha^\kappa = x_\alpha^\kappa\frac{M^\kappa}{M_\alpha}$ with M^κ as the molar mass of the component and M_α as the average molar mass of the phase. The fluid phase velocity $\mathbf{v}_\alpha$ is determined by Equation 3:

$$\mathbf{v}_\alpha=-\frac{k_{r,\alpha}}{\mu_\alpha}K(\nabla p_\alpha-\rho_\alpha\mathbf{g}). \tag{3}$$

K denotes the intrinsic permeability of the porous medium and $k_{r,\alpha}$ the relative permeability of the phase. μ_α is the dynamic viscosity of the phase and p_α is the phase pressure. Gravity is denoted by the vector $\mathbf{g}$. Within the porous-medium domain, we assume a local thermodynamic equilibrium. The energy balance is defined by:

$$\sum_{\alpha\in\{\mathrm{l,g}\}}\left(\phi\frac{\partial(\rho_\alpha S_\alpha u_\alpha)}{\partial t}+\nabla\cdot(\rho_\alpha h_\alpha\mathbf{v}_\alpha)\right)+(1-\phi)\frac{\partial(\rho_s c_{p,s}T)}{\partial t}-\nabla\cdot(\lambda_{pm}\nabla T)=0. \tag{4}$$

u_α is the internal energy of the phase and h_α the specific enthalpy. Due to the differences in enthalpies of the gaseous and the liquid phase, latent heat of vaporization is included in this approach. The solid part of the porous medium is accounted for by the specific heat capacity $c_{p,s}$ and the density of the solid ρ_s. The thermal conductivity λ_{pm} is a mixture of the thermal conductivities of the liquid and the gaseous and the solid phase and is computed by the Somerton approach (Somerton et al., 1974).

2.2.2. Free-Flow Domain

The free-flow can be described by the Navier-Stokes equations:

$$\frac{\partial\rho_g\mathbf{v}_g}{\partial t}+\nabla\cdot\left(\rho_g\mathbf{v}_g\mathbf{v}_g^T\right)-\nabla\cdot(\boldsymbol{\tau}_g)+\nabla\cdot(p_g\mathbf{I})-\rho_g\mathbf{g}=0. \tag{5}$$

with $\mathbf{I}$ as the identity matrix. The mass balance for each component is given by:

$$\frac{\partial\left(\rho_g X_g^\kappa\right)}{\partial t}+\nabla\cdot\left(\rho_g\mathbf{v}_g X_g^\kappa-\mathbf{j}_{\mathrm{diff}}^\kappa\right)-q^\kappa=0. \tag{6}$$

The diffusive fluxes $\mathbf{j}_{\mathrm{diff}}^\kappa=\mathbf{D}_\alpha^\kappa\rho_\alpha\nabla X_\alpha^\kappa$ are, as in the porous medium, described by Fick's law.

In order to properly describe turbulent free-flow behavior the so-called Reynolds-Averaged Navier-Stokes (RANS) equations are used. This splits the fluctuating terms into averaged and fluctuating values, which introduces a new term, the Reynolds stress tensor $\boldsymbol{\tau}_{g,t}$. The momentum balance can be denoted as:

$$\frac{\partial \rho_g \mathbf{v}_g}{\partial t} + \nabla \cdot \left(\rho_g \mathbf{v}_g \mathbf{v}_g^T\right) - \nabla \cdot (\boldsymbol{\tau}_g + \boldsymbol{\tau}_{g,t}) + \nabla \cdot (p_g \mathbf{I}) - \rho_g \mathbf{g} = 0. \tag{7}$$

As closure relations for the newly introduced Reynold's stress $\boldsymbol{\tau}_{g,t} = \mu_{g,t}\left(\nabla \mathbf{v}_g + \nabla \mathbf{v}_g^T\right) - \left(\frac{2}{3}\rho_g k \mathbf{I}\right)$ in this work a $k-\omega$ turbulence model is used. More information about this can be found in Wilcox (2008).

The mass balance equation for the transport of a component in the free-flow is given with:

$$\frac{\partial\left(\rho_g X_g^\kappa\right)}{\partial t} + \nabla \cdot \left(\rho_g \mathbf{v}_g X_g^\kappa - \mathbf{j}_{\text{diff},t}^\kappa\right) - q^\kappa = 0. \tag{8}$$

where the turbulent diffusion $\mathbf{j}_{\text{diff},t}^\kappa$ uses an effective diffusion coefficient that also accounts for turbulent behavior with: $D_{\text{eff},t}^{ij} = D_g^{ij} + D_t$. D_t is the eddy diffusivity.

The energy balance can be described with:

$$\frac{\partial(\rho_g u_g)}{\partial t} + \nabla \cdot (\rho_g h_g \mathbf{v}_g) + \sum_i \nabla \cdot \left(h_g^\kappa \mathbf{j}_{\text{diff},t}^\kappa\right) - \nabla \cdot ((\lambda_g + \lambda_t)\nabla T) = 0, \tag{9}$$

where the λ_t is the eddy conductivity. More information about these models can be found in for example, Fetzer et al. (2016).

2.2.3. Interface Coupling Conditions

The interface conditions are based on the assumption of local thermodynamic equilibrium (Mosthaf et al., 2011). At the interface, we assume that temperatures, the pressure and mole fractions are equal. Continuity of fluxes at the interface is then described by:

$$\left[(\rho_g \mathbf{v}_g) \cdot \mathbf{n}\right]^{\text{ff}} = -\left[(\rho_g \mathbf{v}_g + \rho_w \mathbf{v}_w) \cdot \mathbf{n}\right]^{\text{pm}}. \tag{10}$$

The tangential component of the momentum balance is set to the Beavers-Joseph-Saffman condition (Beavers & Joseph, 1967; Jones, 1973; Saffman, 1971), describing the slip velocity at the interface.

$$\left[\left(-\mathbf{v}_g - \frac{\sqrt{(\mathbf{K}\mathbf{t}_i)\cdot \mathbf{t}_i}}{\alpha_{BJ}}\left(\nabla \mathbf{v}_g + \nabla \mathbf{v}_g^T\right)\mathbf{n}\right) \cdot \mathbf{t}_i\right]^{\text{ff}} = 0, \quad i \in \{1, .., d-1\}. \tag{11}$$

For the normal part of the momentum coupling condition, we use a continuity of normal stresses.

$$\left[\left(\left(\rho_g \mathbf{v}_g \mathbf{v}_g^T - (\boldsymbol{\tau}_g + \boldsymbol{\tau}_{g,t}) + p_g \mathbf{I}\right)\mathbf{n}\right)\right]^{\text{ff}} = \left[(p_g \mathbf{I})\mathbf{n}\right]^{\text{pm}}. \tag{12}$$

For a component, i, continuity of fluxes is written as:

$$\left[\left(\rho_g X_g^\kappa \mathbf{v}_g + \mathbf{j}_{\text{diff},t}\right) \cdot \mathbf{n}\right]^{\text{ff}} = -\left[\left(\sum_\alpha \left(\rho_\alpha X_\alpha^\kappa \mathbf{v}_\alpha + \mathbf{j}_{\text{diff},\alpha}^\kappa\right)\right) \cdot \mathbf{n}\right]^{\text{pm}}. \tag{13}$$

For the energy coupling the flux condition is:

$$\left[\left(\rho_g h_g \mathbf{v}_g + \sum_i h_g^\kappa \mathbf{j}_{\text{diff},g}^\kappa + \lambda_g \nabla T\right) \cdot \mathbf{n}\right]^{\text{ff}} = -\left[\left(\sum_\alpha \left(\rho_\alpha h_\alpha \mathbf{v}_\alpha + \sum_i h_\alpha^\kappa \mathbf{j}_{\text{diff},\alpha}^\kappa\right) - \lambda_{\text{pm}} \nabla T\right) \cdot \mathbf{n}\right]^{\text{pm}}. \tag{14}$$

2.3. Numerical Model

The porous-medium domain is discretized using cell-centered finite volumes. The simulations were performed using a two-point flux approximation on a rectangular grid. The free-flow domain is also discretized using finite volumes but with the marker and cell scheme. More details are described in Coltman et al. (2020).

The above-mentioned concepts are implemented using the open-source simulation environment DuMu^x (Flemisch et al., 2011; Koch et al., 2021), which is based on the open-source numerical toolbox DUNE. The source code for the below-performed simulations is accessible via a DuMu^x publication module (https://git.iws.uni-stuttgart.de/dumux-pub/kiemle2022a) and via the data repository of the University of Stuttgart (DaRUS; Kiemle & Heck, 2022b).

3. Simulation Scenario

In our analysis, we investigate the fractionation behavior of the heavy water isotopologues $^2H^1HO$ and $H_2^{18}O$ in relation to ordinary water $H_2^{16}O$ during an evaporation process.

Usual methods to validate the isotopic fractionation process, as presented in Braud et al. (2005) or Zhou et al. (2021), cannot be applied to our model. The validation through the analytical solution by Barnes and Allison (1983) is not applicable as this solution is derived for a constant evaporation rate without resolving a free-flow domain and applying parameterization for the kinetic fractionation. The verification through an experimental comparison is restricted by the need for an exact description of the free-flow domain, with a controlled climate and wind speed. This is why we create a virtual evaporation experiment in which a fully saturated soil column dries out under constant atmospheric conditions. With this model setup, we present the ability of our model to simulate isotopic fractionation during evaporation and are able to analyze the physical behavior.

- Scenario 1 (Section 4.1): Here, we employ laminar conditions in the free-flow domain. This scenario is used to present that our model is able to simulate isotopic fractionation processes.
- Scenario 2 (Section 4.2): The laminar free-flow conditions are kept, but single parameters which influence the fractionation behavior are isolated. This approach has been proposed by Mathieu and Bariac (1996) to verify if the model reproduces reasonable results for each parameter influencing the fractionation process. The study has been conducted under isothermal conditions ($T = 289$ K).
- Scenario 3 (Section 4.3): Finally, we enable turbulent conditions in the free-flow domain. This scenario should give an impression on the options of modeling the free-flow and coupling the free-flow and the porous medium available in DuMu^x, and how these options can be used to further investigate fractionation processes in at soil-atmosphere interface.

The setup comprises a wind tunnel with a flat porous medium beneath. The wind velocity profile develops from the left to the right side from a parabolic-shaped profile into a fully developed velocity profile. From the left side, the free-flow domain is constantly supplied with stable water isotopologues and water vapor. Figure 2 shows a sketch of the initial and boundary conditions of the simulation setup. As this evaluation does not include any specific pore scale information, the Beavers-Joseph coefficient α_{BJ}, used in the tangential momentum coupling condition, is set to 1.

Inside the porous-medium domain, we set the properties to match a light clay (Yolo light clay [Moore, 1937]) with a texture of 31.2% clay, 45.0% silt and 23.8% sand for our simulations. The spatial parameters of the soil are listed in Table 1.

The applied fluid system comprises the components air, $H_2^{16}O$, $^2H^1HO$ and $H_2^{18}O$. The non-isotopic properties and relationships of our fluid system can be found in IAPWS (2007), as well as in the DuMu^x documentation and in the DuMu^x publication module (Kiemle & Heck, 2022b). The binary liquid diffusion coefficient for "$H_2^{16}O$ - isotopologue" is proportional to the liquid self-diffusion coefficient of $H_2^{16}O$. The proportional factor can be found in Mathieu and Bariac (1996). The diffusion between air-isotopologues in the vapor phase was defined by using the gas diffusion coefficient of $H_2^{16}O$-Air and a proportional factor given by Merlivat (1978). The isotopic vapor pressure (see Equation 1) was defined by using coefficients proposed by Van Hook (1968). A detailed overview of these parameters used in our model can be found in the Appendix A.

The composition of isotopologues is commonly written in the δ-notation that relates the ratio of isotopologues to ordinary water to a standard value: $\delta_\alpha^i = \frac{R_\alpha^i - R_{V-SMOW}}{R_{V-SMOW}} \cdot 1{,}000\ [‰]$ with $R_\alpha^i = \frac{N^i}{N^{H_2^{16}O}}$ and R_{V-SMOW} the standard

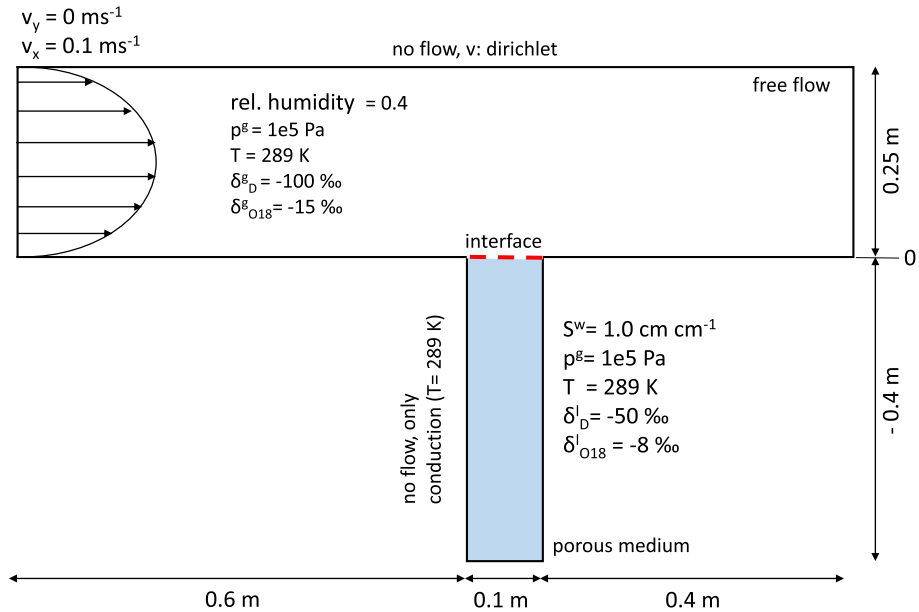

Figure 2. Initial and boundary conditions for analyzing stable water isotopic fractionation during evaporation. The problem is discretized using 100 cells/m in the vertical direction and with 400 cells/m (porous-medium domain) and 100 cells/m (free-flow domain) in the horizontal direction. A vertical grid refinement toward the interface region is used. Initially, the porous-medium domain is uniformly saturated, and the isotopologues are equally distributed.

mean ocean water (Gonfiantini, 1978). Concerning the δ-notation, the superscript i describes only the heavier atom of the isotopologue instead of the entire molecule.

4. Results and Discussion

4.1. Water Isotopologue Transport Under Laminar Flow Conditions

We focus on the fractionation behavior in the porous-medium domain during the evaporation of a soil column. As described in Section 2.1, we expect an enrichment of isotopologues toward the evaporation front in the porous-medium domain caused by the equilibrium fractionation in the saturated zone and subsequently a decrease in the isotopic composition caused by intrusion of the isotopic-depleted atmosphere in the dried porous-medium zone. Thus, the resulting isotope profile remains constant in the saturated zone (no fractionation) but forms a peakshape at the evaporation front.

Table 1
Spatial Parameters of Yolo Light Clay

Parameter	Value
Porosity ϕ	0.35
Permeability K	1.23E-14 m^2
Residual saturation of non-wetting phase S_{nr}	0.00
Residual saturation of wetting phase S_{wr}	0.00
Van Genuchten parameter n	2.221
Van Genuchten parameter α	0.0005 Pa^{-1}
Solid density ρ_s	1,300 kg m^{-3}
Solid thermal conductivity λ_s	0.5 W m^{-1}K^{-1}
Solid heat capacity $c_{p,s}$	1,300 J kg^{-1}K^{-1}

As a first step, we set up a stable water isotopologue transport problem with laminar flow (v_x = 0.1 m/s) above the porous-medium domain. Here, the focus is placed on the isotope fractionation process itself without the influence of turbulent mixing in the free-flow. In Figure 3, the isotopic compositions for various days are plotted as (a) vertical and (b) horizontal profiles. In the vertical profiles, it can be observed that the simulated profiles match the theoretical description depicted in Figure 1. Both, the isotopic enrichment toward the evaporation front and the depletion in the dry domain of the porous medium are simulated. Further, we observe how the soil column dries out over time as the evaporation front propagates downwards. The drying of the soil and so the evaporation front can be retraced by the corresponding saturation and temperature profiles (Appendix B: Figure B1).

In the horizontal profiles, the spatial distribution across the x-axis of the isotopologues and their fractionation behavior is visible. As the flow profile is developed from the left side and we consider conduction at all boundaries of the porous-medium domain, a spatial variation in isotopic composition can

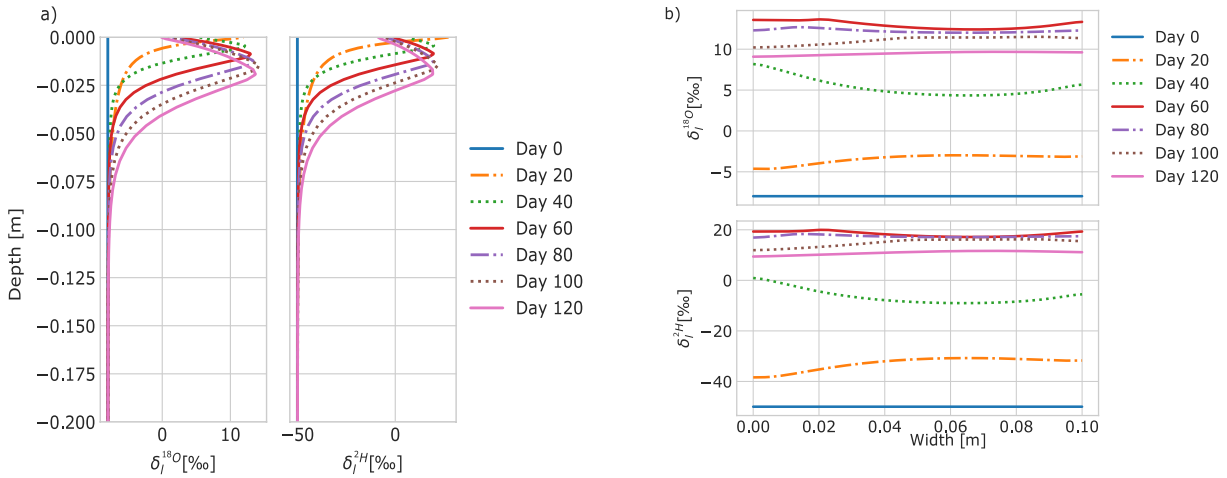

Figure 3. Isotopic composition δ_l^i over time. (a) Vertical liquid water isotope composition profiles in the middle of the soil column (at 0.05 m width) at selected days; (b) horizontal liquid water isotope composition profiles at −0.01 m soil column depth at selected days.

be observed. As seen in the vertical isotopic profiles, the isotopic species are either enriched or depleted in the porous-medium domain. During stage-I evaporation, the isotopologues enrich over the whole column width. As evaporation progresses, the upper layers of the porous-medium domain dry completely, and the isotopologues are depleted because the influence of the atmosphere with low isotopic concentration increases.

In our study, we analyze how the different stages of evaporation influence the enrichment of the water isotopologues. In Figure 4, the temporal isotopic composition and the liquid saturation evolution for different soil column depths and the corresponding evaporation rate are plotted. We can see that during stage-I evaporation, where evaporation rates are higher, the isotopic composition first enriches before depletion. This enrichment peak is here referred to as "stage-I peak." Afterward, during the transition to stage-II evaporation, we observe another peak in isotopologue composition, which we refer to as "stage-II peak."

During stage-I evaporation, the isotopologues first enrich due to their lower vapor pressure relative to ordinary water. As the soil begins to dry, the isotopic composition decreases as isotopologue-depleted air from the atmos-

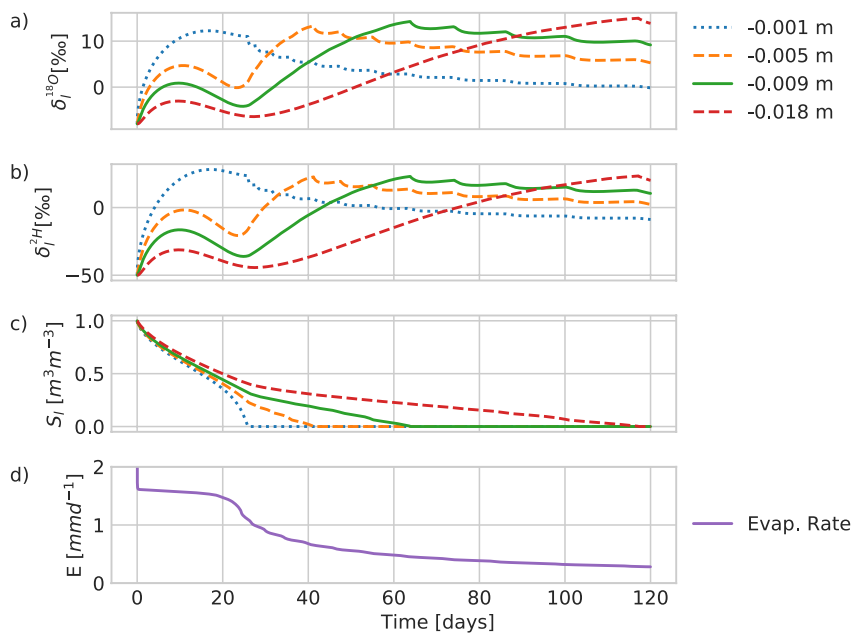

Figure 4. Influence of evaporation behavior on the isotopic fractionation process in different soil column depths over time. (a, b) Isotopic composition δ_l^i; (c) liquid phase saturation; (d) evaporation rate over a 120 days period.

Table 2
Parameter Change for Fractionation Process Study

Case	Description	Gas pressure p^i	Gas diffusion coeff. $D_g^{i,air}$	Liq. diffusion coeff. $D_l^{H_2O,i}$	Mole fraction in Ω_{ff}
1	No fractionation	p^{H_2O}	$D_g^{H_2O,air}$	$D_l^{H_2O,self}$	$x^i_{g,ff} = x^i_{g,pm}$
2	Only equilibrium fractionation	p^i	$D_g^{H_2O,air}$	$D_l^{H_2O,self}$	$x^i_{g,ff} = x^i_{g,pm}$
3	Only kinetic fractionation	p^{H_2O}	$D_g^{i,air}$	$D_l^{H_2O,self}$	$x^i_{g,ff} = x^i_{g,pm}$
4	Only liquid diffusion	p^{H_2O}	$D_g^{H_2O,air}$	$D_l^{H_2O,i}$	$x^i_{g,ff} = x^i_{g,pm}$
5	Reference	p^i	$D_g^{i,air}$	$D_l^{H_2O,i}$	$x^i_{g,ff} < x^i_{g,pm}$

phere intrudes into the drying soil. At a certain state of drying the porous medium reaches the residual saturation. The evolution of the dry zone for our scenario can be traced in Figure 4c. With no mobile liquid water at the surface, further evaporation is limited by vapor transport in the gas phase. Compared to before, isotopic species are enriching again, leading to a second peak. In this stage, the intrusion of air from the atmosphere is decreasing, as the air volume in the porous medium does not change much anymore. However, lighter water isotopologues are still evaporating from the remaining liquid water, resulting in an increase in the isotopic composition. This leads to the second peak, the "stage-II peak." When drying further, eventually the water saturation reaches zero and the isotopologue composition decreases again.

These peaks in isotopologue composition are also described in various other modeling studies, for example, for unsaturated soils by Barnes and Allison (1983). In their study they consider a soil with a dry layer on top, that is dominated by vapor transport. This described peak corresponds to our "stage-II peak" mentioned in this work.

In Figure 4, we show that the isotopic composition over time for various depths can be used to gain further insights into the evaporation and isotopologue transport processes. In the first soil layer, we only observe a stage-I peak. As this cell is located at the interface, the cell directly dries out when the atmospheric demand can no longer be supplied. In the other depths, the impact of the transition between stage-I and stage-II evaporation becomes more visible. However, with increasing soil depths, the evolution of the stage-I peak becomes less dominant as soils further from the surface are less impacted by the atmospheric evaporation demand.

4.2. Study of Fractionation Process

Mathieu and Bariac (1996) proposed a qualitative study to verify the isotopic enrichment of their isotope transport model. The aim of this study is to check on the influencing fractionation parameters by isolating each specific parameter. In Table 2, the isolated parameters used in the model for this process study are summarized.

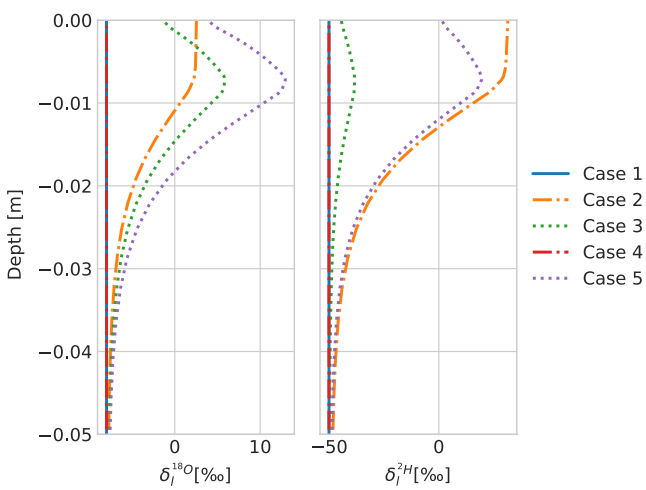

Figure 5. Process behavior of isolated parameters that influence the isotopic fractionation at 50 days. Isotopic composition δ_l^i of ordinary water and its isotopes.

In Figure 5, the results of our fractionation study are displayed. The fractionation process is analyzed for the vertical isotope profiles for $^2H^1HO$ and $H_2^{18}O$. The study cases are performed with the same model setup as described in Section 3 and with the same drying conditions ($v_x = 0.1$ m/s, 50 days period). In the Appendix B (Figure B2), the corresponding mole fraction profiles of water and its isotopologues in the liquid phase are plotted to enhance our understanding of fractionation processes.

- **Case 1 - No isotopic fractionation:** All factors which lead to isotopic fractionation (vapor pressure difference, liquid and gaseous diffusion coefficients, isotopic composition gradient between free-flow and porous-medium domain) are neglected. Hence, no significant fractionation compared to the initial state is obtained (max. deviation for $H_2^{18}O$ < 0.199% and for $^2H^1HO$ < 0.030%). As we are observing an evaporation process, a concentration gradient toward the soil surface is formed (vapor zone). However, as water and its isotopes are both evaporating with the same slope, the isotopic composition remains constant.

- **Case 2 - Only equilibrium fractionation:** The equilibrium fractionation factor describes the tendency of a component to separate from a mixture. By enabling the difference in vapor pressure of the isotopes, the equilibrium fractionation is reintroduced ($p_g^{H_2^{16}O}$ = 1801.4 Pa, $p_g^{^2H^1HO}$ = 1659.88 Pa, $p_g^{H_2^{18}O}$ = 1782.51 Pa). The isotopologues enrich toward the evaporation front due to phase equilibrium conditions. In the vapor zone, the composition remains nearly constant since there is no transport in the liquid phase anymore once the residual saturation is reached. Nearly fully dried, the influence of equilibrium fractionation is greatly reduced. In our case, $^2H^1HO$ is more likely to partition from ordinary water than $H_2^{18}O$ ($\beta_{eq}^{^2H^1HO}$ = 0.921, $\beta_{eq}^{H_2^{18}O}$ = 0.990).
- **Case 3 - Only kinetic fractionation:** Compared to Case 1, the binary gas diffusion coefficient is reintroduced for the isotopologues ($D_g^{H_2^{16}O,air}$ = 2.36e^{-5}m^{2}s^{-1}, $D_g^{^2H^1HO,air}$ = 2.30 e^{-5}m^{2}s^{-1}, $D_g^{H_2^{18}O,air}$ = 2.29 e^{-5}m^{2}s^{-1}). Enabling the gas diffusion coefficient leads to an increase of the isotopic composition in the unsaturated zone as the isotopologues diffuse slower due to the lower diffusion coefficient, and subsequently to a decrease in the gaseous zone toward the isotopic-depleted free-flow concentration.
- **Case 4 - Only liquid diffusion coefficient:** The liquid diffusion coefficient of the isotopologues is proportional to the self-diffusion coefficient of pure water ($D_l^{H_2^{16}O,i} = a^i\ D_l^{H_2^{16}O,self}$ [Mathieu & Bariac, 1996]). As the liquid diffusion may influence the mixing behavior of the isotopologues in the saturated and unsaturated zone, we isolate the liquid diffusion coefficient instead of only using the self-diffusion coefficient of water for the isotopic species ($D_l^{H_2^{16}O,self}$ = 1.819 e^{-9}m^{2}s^{-1}, $D_l^{^2H^1HO}$ = 1.789 e^{-9}m^{2}s^{-1}, $D_l^{H_2^{18}O}$ = 1.759 e^{-9}m^{2}s^{-1}). The liquid diffusion coefficient itself does not majorly affect the fractionation process as the advective term in the mass balance (capillary uptake) dominates the mixing and flow process in this case (compared to the initial state max. deviation for $H_2^{18}O < 0.122\%$ and for $^2H^1HO < 0.019\%$).
- **Case 5 - Reference:** As a reference, we enable all factors leading to fractionation. The results show both, a high enrichment toward the evaporation front (as in Case 2) and a depletion toward the soil surface (Cases 3 + 4).

4.3. Variation of Free-Flow Domain Model

In the previous sections, investigations have been focused on laminar flow problems. However, when considering realistic atmospheric conditions with higher wind velocities, turbulent flow conditions must be regarded as well. As stated above, many studies have been focused on integrating turbulent mixing into the isotopic fractionation process by adapting the kinetic fractionation factor (e.g., Quade et al., 2018). By changing our free-flow - porous medium coupled transport model by using the RANS equations and choosing a $k-\omega$-model turbulence model as described in Section 2 and in Coltman et al. (2020) and Heck et al. (2020), the evaporation is affected leading to different fractionation processes compared to laminar flow assumptions.

The velocity profile in the free-flow domain evolves from left to right from a block velocity profile to a fully developed flow profile for turbulent flow. For the laminar cases, a parabolic velocity profile is set on the left side, and from that, the flow profile develops. In Figure 6, the different flow scenarios are schematically displayed. The different flow scenarios affect the diffusive flux near the interface, which further influences the evaporation rate at the soil surface (Figure 7) and so the isotopic composition inside the porous medium (Figure 8). As we want to show the variety of our free-flow model, we chose realistic flow scenarios for our laminar and turbulent flow cases. Since laminar flow mostly occurs indoors or under controlled conditions the boundary conditions for the laminar case resemble a wind tunnel. As isotopic fractionation is an environmental issue, we are also interested in outdoor conditions. Therefore, we choose the turbulent case boundary conditions which are suitable to replicate outdoor conditions, without a closed top at the upper boundary.

For our analysis of the influence of different flow conditions on isotopic composition, we test different free-flow velocities (Table 3). The turbulent flow problems result in different evaporation rates and evaporation profiles (Figure 7), as the maximum evaporation rate is higher and the duration of stage-I is shortened by increasing the flow velocity.

In the previous section, we hypothesized that the stage of evaporation (stage-I/stage-II) will have a crucial influence on the isotopic fractionation behavior in the porous medium. Thus, we analyze the isotopic distribution (in the vertical and horizontal direction) during different evaporation states and for different velocities (Figure 8).

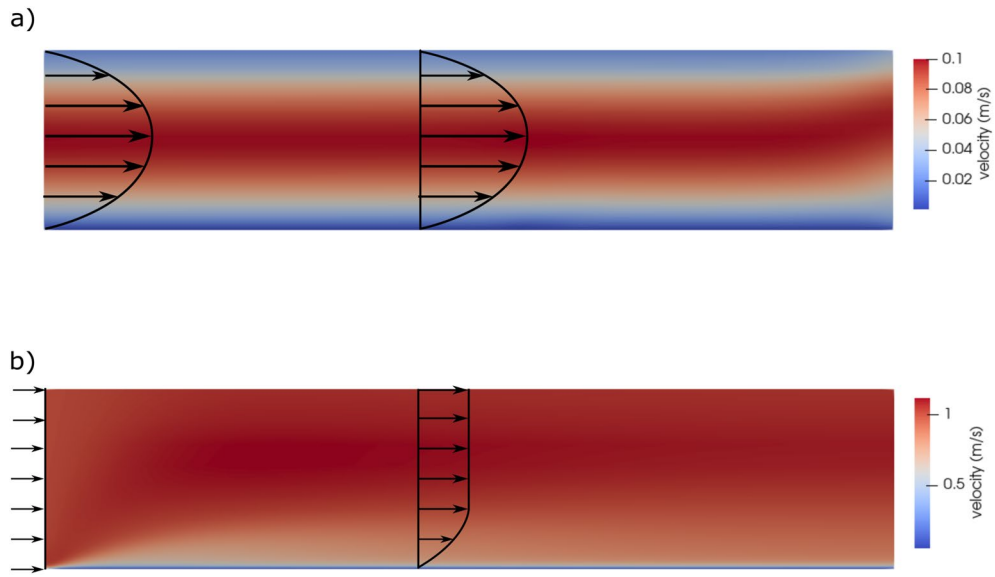

Figure 6. Influence of the boundary layer thickness developed by (a) laminar, (b) turbulent flow on mass transfer at the interface. We assume that the mass transfer is limited at the interface region, boundary layers form based on the present flow type and that outside the formed boundary layer the flow is fully mixed.

We compare the different flow cases among each other during stage-I and stage-II and for the transition zone between those stages. With this in mind, simulation times are selected such that all cases reached similar evaporation stages. However, due to the great difference in evaporation rates, it is not possible to separate the stages for all cases completely. In order to make conclusions about the role of temperature and saturation the temporal evolution of these parameters at the top of the soil column is attached (Appendix B: Figure B3).

4.3.1. Vertical Isotopic Distribution

- **Stage-I Evaporation:** In this stage, isotopic fractionation is characterized by equilibrium fractionation. In this stage, both the laminar and the turbulent flow problems show a similar behavior. Both flow scenarios enrich toward the soil surface. However, compared to the turbulent flow, the laminar cases enrich less toward the soil surface. If the laminar and the turbulent cases are compared among themselves, it can be observed that the variation in wind speed affects the laminar cases more than the turbulent cases. This can be observed in the isotopic composition and in the gradient. This is due to the higher evaporation rates seen in the turbulent cases. Thus, the influence of the equilibrium fractionation is reduced and therefore less difference can be seen in the isotopic composition. However, some differences are still visible. The highest velocities lead to the highest enrichment. A reason for this is the different temperatures during stage-I evaporation. Higher evaporation rates lead to substantial evaporative cooling. The equilibrium fractionation process is temperature sensitive, and lower temperatures lead to lower equilibrium fractionation factors which means more partitioning of the isotopologues.
- **Transition:** A mixed representation of different evaporation states is visible at this point in the simulation. Where the laminar cases are still in stage-I evaporation, the turbulent cases are in different stages of the transition into stage-II evaporation. Thus, the interpretation of the turbulence impact on the isotopic composition in this zone is not absolute, but we regard one representative time. However, in all three turbulent cases, we observe that near the soil surface (−0.01 to −0.02 m) the peak in isotopic composition has decreased in comparison with stage-I evaporation.

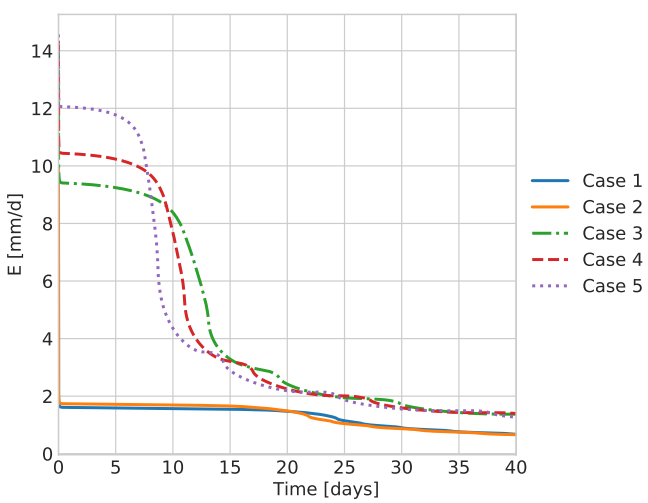

Figure 7. Evaporation rates over time for turbulent (dashed) and laminar (straight) flow problems.

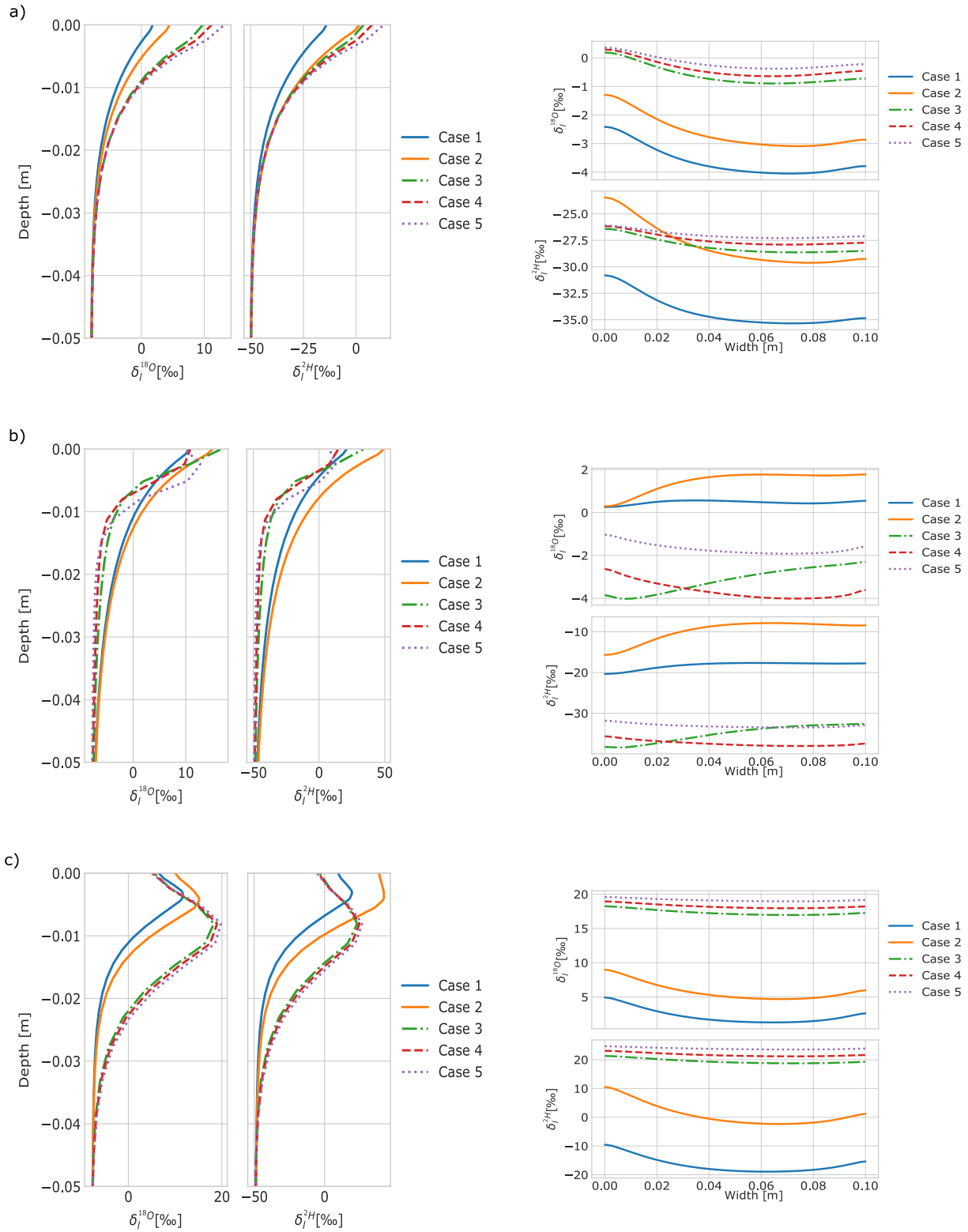

Figure 8. Spatial isotopic composition in the porous-medium domain for different flow problems (Laminar: Cases 1, 2 (solid lines); Turbulent: Cases 3–5 (dashed lines)). Shown are vertical ($x = 0.05$ m) and horizontal ($y = 0.39$ m) isotopic profiles for different evaporation states. (a) Stage-I evaporation ($t = 2$ days), (b) Transition evaporation ($t = 10$ days), (c) Stage-II evaporation ($t = 35$ days).

Table 3
Turbulence Parameter

Case	Conditions	Flow velocity [ms^{-1}]	Reynolds number [-]
1	Laminar	0.1	$Re_D = 1{,}678$
2	Laminar	0.13	$Re_D = 2{,}181$
3	Turbulent	0.5	$Re_L = 2.01e4$
4	Turbulent	1.0	$Re_L = 4.03e4$
5	Turbulent	3.0	$Re_L = 1.21e5$

Note. For parabolic flow profiles, the characteristic length of the Reynolds number (Re_D) is the diameter of the wind tunnel ($d = 0.25$ m) and for initial block profile flow (Re_L), we use the length between the starting point of the free-flow domain and the porous-medium domain ($l = 0.6$ m).

While in the transition zone, the soil temperature raises again due to lower evaporation rates and less evaporative cooling. Then the equilibrium fractionation does not affect the isotopic composition that much anymore and kinetic fractionation becomes more dominant.

Since the laminar cases are still in stage-I evaporation, the isotopic fractionation behavior remains similar to the previous stage. However, one may notice that the surface isotopic composition is increased as was observed in the turbulent cases (see Figure 8a). The wind velocities affect the speed of enrichment at the soil surface and the drying of the porous medium but do not significantly affect the maximum isotopic composition at the surface.

- **Stage-II Evaporation:** Here, all cases are in stage-II evaporation and all cases have developed the characteristic peak of the isotopologues. The turbulent cases show a similar behavior. Only minor deviations in the maximal enrichment are visible. For laminar flow, we observe that the maximum enrichment is greater for higher wind velocities, while the evaporation front is nearly on the same level. Still, higher wind velocities lead to drier soil, which in turn affects the peak in isotopic composition.

4.3.2. Horizontal Isotopic Distribution

The impact of the varied free-flow conditions and the subsurface thermal boundary conditions can be observed by evaluating the spatial distribution of the isotopic composition at different depths parallel to the interface.

The influence of the different wind velocities is visible in terms of the evolution of the isotopic composition. As observed in the vertical profiles, the enrichment in the turbulent cases proceeds faster than in the laminar cases. Again, the influence of the different evaporation stages of the different flow problems is visible. In stage-I and stage-II the isotopic composition increases, whereas the isotopic composition is decreasing in the transition zone. During stage-I and stage-II the isotopic composition of the turbulent cases shows only minor deviations in comparison with the laminar cases. While in the transition zone, in which the evaporation state varies for each case, the spatial distribution of the turbulent cases is also varying considerably. Here, the spatial isotopic composition of a developed evaporation front (Case 5), a forming evaporation front (Case 4), and a surface evaporation front (Case 3) are displayed. Further, the effects of decreasing evaporation rates and less evaporative cooling on the horizontal distribution of the isotopic composition during different evaporation steps can be observed here.

Considering the spatial variation of the isotopic enrichment within the single cases, the one-dimensional assumption is for most cases sufficient. In addition, the applied conduction boundary condition in the porous medium of our virtual case has also a crucial impact on the enrichment of the isotopologues. For special cases, as observed in our laminar cases, a larger change in isotopic composition is possible along the horizontal axis.

5. Summary and Outlook

In this work, we presented a bare soil evaporation and stable water isotopologue transport and mixing scenario which was analyzed using different free-flow conditions. By using appropriate coupling conditions which ensure mass, momentum, and energy transfer across the free-flow and porous medium domain, we were able to simulate fractionation processes which occur due to evaporation from soils.

Considering laminar conditions, it is shown that the coupled model can reproduce the characteristic enrichment peaks in isotopic composition during the evolution of the evaporation front, as well as the depletion of isotopologues in the dry soil during the drying of the soil. Further, a correlation between the isotopic composition and the different stages of evaporation can be observed. In the isotopic composition at certain levels, the impact of the different stages of evaporation is visible as during stage-I a first peak in the isotopic composition is observed and a second peak appears in stage-II evaporation. In an additional study, we test the robustness of our model by separating the processes of equilibrium and kinetic fractionation. The effect of wind velocity and turbulent mixing on the isotopic composition in soil is studied. For that, we use a RANS approach for the description of the turbulent flow in the free-flow. This analysis allows us to further study the influence of the evaporation rate and the evaporation stages on the isotopic composition. The temperature-sensitive equilibrium fractionation is

affected by higher evaporation rates as higher evaporative cooling leads to a higher partitioning of isotopologues. In stage-II evaporation, where the kinetic fractionation is more dominant, we observe a variation in the isotopic compositions of the different flow conditions: The turbulent flow cases have similar characteristic peaks in the isotopic composition, but the laminar flow cases show a greater influence of the wind velocity on the isotopic transport.

With the coupled model concept presented in this work, the transport and mixing of stable water isotopologues during soil-water evaporation can be described. We solve transport equations for ordinary water, its isotopologues, and dry air in the porous medium and the free-flow and use suitable coupling conditions to describe the mass, momentum, and energy conservation between the domains. Information about fractionation processes within soils can be derived without the need of using parameterized factors which account for the fractionation process, as used in other existing models. Thus, the coupled transport model can be used as a supportive tool to further specify the parameterization of fractionation processes (especially for the kinetic fractionation at the free-flow - porous medium interface). Note, that besides the absence of parameterizations to describe the fractionation processes, our model relies on equations that have some limitations and assumptions, for example, the choice of suitable coupling conditions (Coltman et al., 2020; Yang et al., 2018). The presented model can be used to further analyze specific parameters which are known for having an influence on the fractionation and evaporation behavior (e.g., degree of soil saturation, soil texture, and atmospheric conditions) and thereof support experimental findings and extend known fractionation factors for 1D simulations or field-scale applications. Here, different concepts for coupling the free-flow and the porous medium, but also for modeling different turbulent free-flow scenarios are available in the simulation environment DuMu^{x}.

Further, the presented model can be expanded for various scenarios and realistic conditions, such as surface topology (Coltman et al., 2020), radiation (Heck et al., 2020) or precipitation (without surface run-off) and inflow events. The coupling of the free-flow and the porous medium domain also allows us to use atmospheric measurements (which are often conducted 2 m above the soil surface) and account for the convective transport in the free-flow region. Thus, in future work, we can validate our model using field-scale lysimeter experiments. Additionally, the presence of salt concentration in soil waters affects the evaporation rate and so the fractionation process (Sofer & Gat, 1975), as salt precipitation and concentration instabilities occur during the evaporation process in the porous medium (Shokri-Kuehni et al., 2020). The effect of salinity on the fractionation process could be further investigated in the context of this model.

Appendix A: Isotopologue Specific Parameters

Equations A1–A3 describe the binary diffusion coefficients for the isotopologues in the gas $D_g^{Air,i}$ and the liquid phase $D_l^{H_2^{16}O,i}$ in m^2s^{-1}. $D_g^{H_2^{16}O,Air}$ (m^2s^{-1}) refers as the binary gas diffusion coefficient of $H_2^{16}O$-air, T (K) denotes the temperature and p (Pa) describes the gas pressure.

Table A1 provides the isotopologue-specific parameters used in Equations A1–A3 and which have been mentioned in Section 3. Further, the table informs about the isotopologue-specific parameter described in Section 2.1.

$$D_g^{Air,i} = \frac{D_g^{H_2^{16}O,Air}}{b_i} \tag{A1}$$

$$D_g^{H_2^{16}O,Air} = 2.17 \cdot 10^{-5} \frac{1e5}{p} \frac{T}{273.15}^{1.88} \tag{A2}$$

$$D_l^{H_2^{16}O,i} = a_i \cdot 10^{-9} \exp\left(-\left(\frac{-535400}{T^2} + \frac{1393.3}{T} + 2.1876\right)\right) \tag{A3}$$

Table A1
Isotopic Parameter Definitions for Diffusion Coefficients and Vapor Pressures

Parameter definition	Parameter name	Value
Binary liquid diffusion coefficient for "$H_2^{16}O$ - i"	Mathieu and Bariac (1996)	
Proportional factor	$a_{H_2^{18}O}$	0.9669
Proportional factor	$a_{^2H^1HO}$	0.9833
Binary gaseous diffusion coefficient for "air - i"	Merlivat (1978)	
Proportional factor	$b_{H_2^{18}O}$	1.0285
Proportional factor	$b_{^2H^1HO}$	1.0251
Isotopic vapor pressure coefficients	Van Hook (1968)	
$H_2^{18}O$		
	A	1,991.1
	B	−4.1887
	C	0.001197
$^2H^1HO$		
	A	26,398.8
	B	−89.6065
	C	0.075802

Appendix B: Additional Results of Numerical Analysis

In the following, we present additional numerical results which support the understanding and the findings in Section 4. Figure B1 represents the saturation and temperature profiles accomplishing the isotope profiles in Figure 3. The qualitative study presented in Section 4.2 is reinforced by the corresponding mole fractions (Figure B2). The findings of Section 4.3 are accompanied by temperature and saturation profiles at the top of the sand column in order to make this more relatable to the respective evaporation rate. Figure B3 represents these values over time.

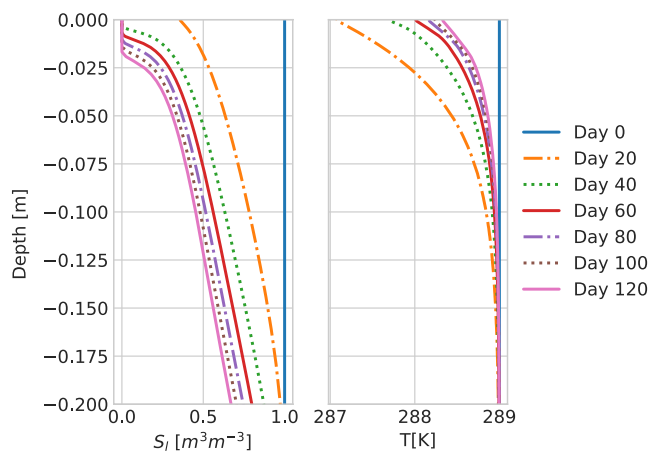

Figure B1. Vertical liquid saturation and temperature profiles for different simulation days for laminar flow scenario 1 in correspondence to Figure 3.

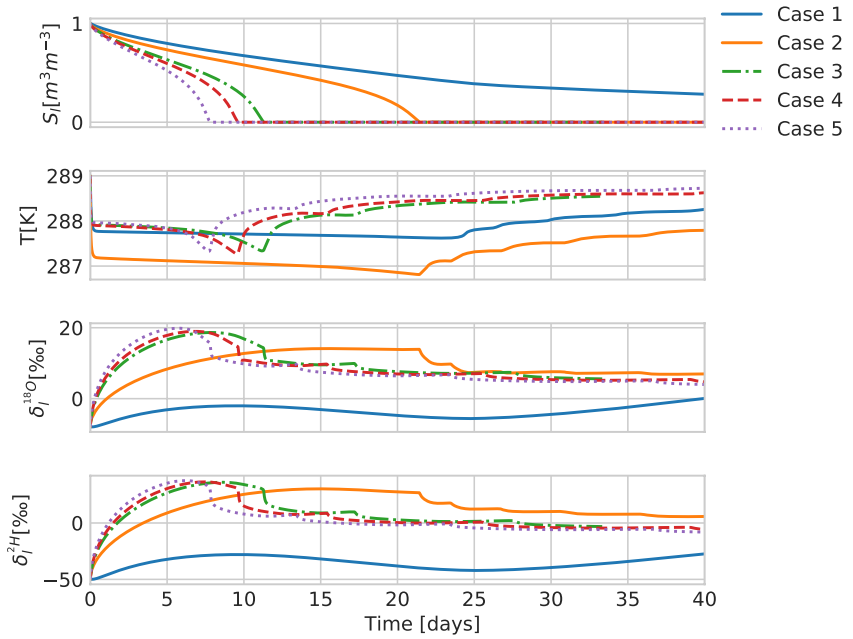

Figure B3. Temporal liquid saturation, temperature and isotopic composition δ_l^i progression at the top of the soil column (−0.001 m) for different flow problems (Laminar: Cases 1, 2 (solid lines); Turbulent: Cases 3–5 (dashed lines)).

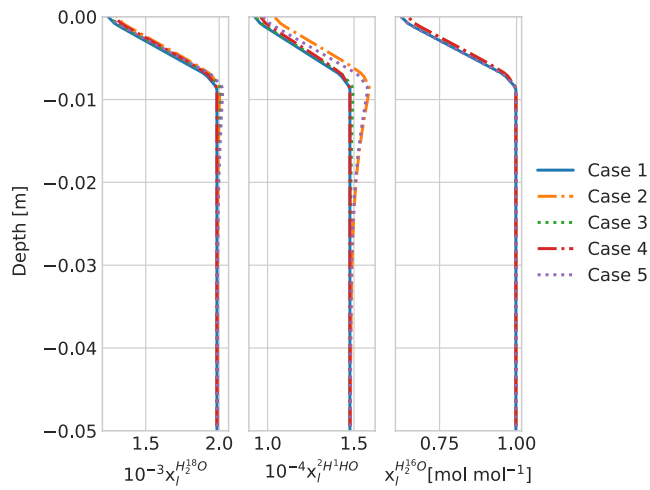

Figure B2. Process behavior of isolated fractionation parameter at 50 days. Corresponding mole fraction x_l^i of ordinary water and its isotopic species to the fractionation process study shown in Figure 5.

Data Availability Statement

All code relevant to obtaining the numerical examples is implemented in DuMu^x (Koch et al., 2021) and can be found under Gitlab (git.iws.uni-stuttgart.de/dumux-pub/Kiemle2022a). Additionally, the code and the numerical data set to reproduce the results are available in the data repository of the University of Stuttgart (DaRUS) and can be accessed via the following sources: Kiemle and Heck (2022a) (numerical data set), Kiemle and Heck (2022b) (code).

Acknowledgments
The authors thank the Deutsche Forschungsgemeinschaft (DFG, German Research Foundation) for supporting this work by funding SFB 1313, Project Number 327154368 and the DFG Research Group Satin 2531/14-1. The authors also thank the DFG for supporting this work by funding SimTech via Germany's Excellence Strategy (EXC 2075 – 390740016). Open Access funding enabled and organized by Projekt DEAL.

References

Aleinov, I., & Schmidt, G. (2006). Water isotopes in the GISS modelE land surface scheme. *Global and Planetary Change*, *51*(1–2), 108–120. https://doi.org/10.1016/j.gloplacha.2005.12.010

Barnes, C., & Allison, G. (1983). The distribution of deuterium and ^{18}O in dry soils: 1. Theory. *Journal of Hydrology*, *60*(1–4), 141–156. https://doi.org/10.1016/0022-1694(83)90018-5

Barnes, C., & Allison, G. (1984). The distribution of deuterium and ^{18}O in dry soils: 3. Theory for non-isothermal water movement. *Journal of Hydrology*, *74*(1–2), 119–135. https://doi.org/10.1016/0022-1694(84)90144-6

Beavers, G. S., & Joseph, D. D. (1967). Boundary conditions at a naturally permeable wall. *Journal of Fluid Mechanics*, *30*(1), 197–207. https://doi.org/10.1017/s0022112067001375

Braud, I., Bariac, T., Gaudet, J. P., & Vauclin, M. (2005). SiSPAT-Isotope, a coupled heat, water, and stable isotope (HDO and $H_2{}^{18}O$) transport model for bare soil. Part I. Model description and first verifications. *Journal of Hydrology*, *309*(1–4), 277–300. https://doi.org/10.1016/j.jhydrol.2004.12.013

Brutsaert, W. (1975). The roughness length for water vapor sensible heat, and other scalars. *Journal of the Atmospheric Sciences*, *32*(10), 2028–2031. https://doi.org/10.1175/1520-0469(1975)032⟨2029:TRLFWV⟩2.0.CO;2

Coltman, E., Lipp, M., Vescovini, A., & Helmig, R. (2020). Obstacles, interfacial forms, and turbulence: A numerical analysis of soil-water evaporation across different interfaces. *Transport in Porous Media*, *134*(2), 134–301. https://doi.org/10.1007/s11242-020-01445-6

Craig, H. (1961). Isotopic variations in meteoric waters. *Science*, *133*(3465), 1702–1703. https://doi.org/10.1126/science.133.3465.1702

Craig, H., & Gordon, L. I. (1965). *Deuterium and oxygen 18 variations in the ocean and marine atmosphere*. Consiglio Nazionale Delle Richerche, Laboratorio de Geologia Nucleare Pisa.

Dongmann, G., Nürnberg, H. W., Förstel, H., & Wagener, K. (1974). On the enrichment of $H_2{}^{18}O$ in the leaves of transpiring plants. *Radiation and Environmental Biophysics*, *11*(1), 41–52. https://doi.org/10.1007/BF01323099

Fetzer, T., Smits, K. M., & Helmig, R. (2016). Effect of turbulence and roughness on coupled porous-medium/free-flow exchange processes. *Transport in Porous Media*, *114*(2), 395–424. https://doi.org/10.1007/s11242-016-0654-6

Flemisch, B., Darcis, M., Erbertseder, K., Faigle, B., Lauser, A., Mosthaf, K., et al. (2011). DuMux: DUNE for multi-phase, component, scale, physics, flow, and transport in porous media. *Advances in Water Resources*, *34*(9), 1102–1112. https://doi.org/10.1016/j.advwatres.2011.03.007

Gat, J. R. (1971). Comments on the stable isotope method in regional groundwater investigations. *Water Resources Research*, *7*(4), 980–993. https://doi.org/10.1029/WR007i004p00980

Gonfiantini, R. (1978). Standards for stable isotope measurements in natural compounds. *Nature*, *271*(5645), 534–536. https://doi.org/10.1038/271534a0

Haese, B., Werner, M., & Lohmann, G. (2012). Stable water isotopes in the coupled atmosphere-land surface model ECHAM5-JSBACH. *Geoscientific Model Development*, *5*, 3375–3418. https://doi.org/10.5194/gmd-6-1463-2013

Haverd, V., & Cuntz, M. (2010). Soil-litter-iso: A one-dimensional model for coupled transport of heat, water, and stable isotopes in soil with a litter layer and root extraction. *Journal of Hydrology*, *388*(3–4), 438–455. https://doi.org/10.1016/j.jhydrol.2010.05.029

Heck, K., Coltman, E., Schneider, J., & Helmig, R. (2020). Influence of radiation on evaporation rates: A numerical analysis. *Water Resources Research*, *56*(10). https://doi.org/10.1029/2020WR027332

Horita, J., & Wesolowski, D. (1994). Liquid-vapor fractionation of oxygen and hydrogen isotopes of water from the freezing to the critical temperature. *Geochimica et Cosmochimica Acta*, *58*(16), 3425–3437. https://doi.org/10.1016/0016-7037(94)90096-5

IAPWS. (2007). *Revised release on the IAPWS industrial formulation 1997 for the thermodynamic properties of water and steam (Tech. Rep. No. IAPWS R7-97(2012))*. The International Association for the Properties of Water and Steam.

Jiang, Z., Xu, T., Mallants, D., Tian, H., & Owen, D. (2018). Numerical modeling of stable isotope (^2H and ^{18}O) transport in a hydro-geothermal system: Model development and implementation to the guide basin, China. *Journal of Hydrology*, *569*, 93–105. https://doi.org/10.1016/j.jhydrol.2018.11.065

Jones, I. P. (1973). Low Reynolds number flow past a porous spherical shell. *Mathematical Proceedings of the Cambridge Philosophical Society*, *73*(1), 231–238. https://doi.org/10.1017/S0305004100047642

Kiemle, S., & Heck, K. (2022a). *Data set for reproducing plots showing stable water isotopologue transport and fractionation*. DaRUS. https://doi.org/10.18419/darus-3108

Kiemle, S., & Heck, K. (2022b). *Dumux code for modeling stable water isotopologue transport and fractionation*. DaRUS. https://doi.org/10.18419/darus-3105

Koch, T., Gläser, D., Weishaupt, K., Ackermann, S., Beck, M., Becker, B., et al. (2021). DuMux 3—An open-source simulator for solving flow and transport problems in porous media with a focus on model coupling. *Computers & Mathematics with Applications*, *81*, 423–443. https://doi.org/10.1016/j.camwa.2020.02.012

Kraft, P., Vaché, K., & Breuer, L. (2011). CMF: A hydrological programing language extension for integrated catchment models. *Environmental Modeling & Software*, *26*(6), 828–830. https://doi.org/10.1016/j.envsoft.2010.12.009

Kuppel, S., Tetzlaff, D., Maneta, M., & Soulsby, C. (2018). EcH_2O-iso 1.0: Water isotopes and age tracking in a process-based, distributed ecohydrological model. *Geoscientific Model Development*, *11*(7), 3045–3069. https://doi.org/10.5194/gmd-11-3045-2018

Lehmann, P., Assouline, S., & Or, D. (2008). Characteristic lengths affecting evaporative drying of porous media. *Physical Review E—Statistical Physics, Plasmas, Fluids, and Related Interdisciplinary Topics*, *77*(5), 056309. https://doi.org/10.1103/PhysRevE.77.056309

Luz, B., Barkan, E., Yam, R., & Shemesh, A. (2009). Fractionation of oxygen and hydrogen isotopes in evaporating water. *Geochimica Et Cosmochimica Acta*, *73*(22), 6697–6703. https://doi.org/10.1016/j.gca.2009.08.008

Majoube, M. (1971). Fractionnement en oxygène 18 et en deutérium entre l´eau et sa vapeur. *Journal de Chimie Physique*, *68*, 1423–1436. https://doi.org/10.1051/jcp/1971681423

Mathieu, R., & Bariac, T. (1996). An isotopic study (^2H and ^{18}O) of water movements in clayey soils under a semiarid climate. *Water Resources Research*, *32*(4), 779–789. https://doi.org/10.1029/96WR02995

Melayah, A., Bruckler, L., & Bariac, T. (1996). Modeling the transport of water stable isotopes in unsaturated soils under natural conditions: 1. Theory. *Water Resources Research*, *32*(7), 2047–2054. https://doi.org/10.1029/96WR00674

Merlivat, L. (1978). Molecular diffusivities of $H_2{}^{16}O$, $HD^{16}O$, and $H_2{}^{18}O$ in gases. *The Journal of Chemical Physics*, *69*(6), 2864–2871. https://doi.org/10.1063/1.436884

Moore, R. (1937). *Water conduction from shallow water tables*. University of California. https://doi.org/10.3733/hilg.v12n06p383

Mosthaf, K., Baber, K., Flemisch, B., Helmig, R., Leijnse, A., Rybak, I., & Wohlmuth, B. (2011). A coupling concept for two-phase compositional porous-medium and single-phase compositional free-flow. *Water Resources Research*, *47*(10). https://doi.org/10.1029/2011wr010685

Müller, M., Alaoui, A., Kuells, C., Leistert, H., Meusburger, K., Stumpp, C., et al. (2014). Tracking water pathways in steep hillslopes by $\delta^{18}O$ depth profiles of soil water. *Journal of Hydrology*, *519*, 340–352. https://doi.org/10.1016/j.jhydrol.2014.07.031

Quade, M., Brüggemann, N., Graf, A., Vanderborght, J., Vereecken, H., & Rothfuss, Y. (2018). Investigation of kinetic isotopic fractionation of water during bare soil evaporation. *Water Resources Research*, *54*(9), 6909–6928. https://doi.org/10.1029/2018WR023159

Risi, C., Ogée, J., Bony, S., Besson, C., Raz Yaseef, N., Wingate, L., et al. (2016). The water isotopic version of the land-surface model ORCHIDEE: Implementation, evaluation, sensitivity to hydrological parameters. *Journal of Waste Water Treatment & Analysis*, *07*(04). https://doi.org/10.4172/2157-7587.1000258

Rothfuss, Y., Merz, S., Vanderborght, J., Hermes, N., Weuthen, A., Pohlmeier, A., et al. (2015). Long-term and high-frequency non-destructive monitoring of water stable isotope profiles in an evaporating soil column. *Hydrology and Earth System Sciences*, *19*(10), 4067–4080. https://doi.org/10.5194/hessd-12-3893-2015

Saffman, P. G. (1971). On the boundary condition at the surface of a porous medium. *Studies in Applied Mathematics*, *50*(2), 93–101. https://doi.org/10.1002/sapm197150293

Shokri-Kuehni, S. M. S., Raaijmakers, B., Kurz, T., Or, D., Helmig, R., & Shokri, N. (2020). Water table depth and soil salinization: From pore-scale processes to field-scale responses. *Water Resources Research*, *56*(2). https://doi.org/10.1029/2019WR026707

Shurbaji, A.-R. M., & Phillips, F. M. (1995). A numerical model for the movement of H_2O, $H_2{}^{18}O$, and ^2HHO in the unsaturated zone. *Journal of Hydrology*, *171*(1–2), 125–142. https://doi.org/10.1016/0022-1694(94)02604-A

Sofer, Z., & Gat, J. (1975). The isotope composition of evaporating brines: Effect of the isotopic activity ratio in saline solutions. *Earth and Planetary Science Letters*, *26*(2), 179–186. https://doi.org/10.1016/0012-821X(75)90085-0

Somerton, W., Keese, J., & Chu, S. (1974). Thermal behavior of unconsolidated oil sands. *Society of Petroleum Engineers Journal*, *14*(05), 513–521. https://doi.org/10.2118/4506-PA

Sprenger, M., Leistert, H., Gimbel, K., & Weiler, M. (2016). Illuminating hydrological processes at the soil-vegetation-atmosphere interface with water stable isotopes. *Reviews of Geophysics*, *54*(3), 674–704. https://doi.org/10.1002/2015rg000515

Sprenger, M., Tetzlaff, D., Buttle, J., Laudon, H., Leistert, H., Mitchell, C. P., et al. (2018). Measuring and modeling stable isotopes of mobile and bulk soil water. *Vadose Zone Journal*, *17*(1), 170149–170218. https://doi.org/10.2136/vzj2017.08.0149

Uhlenbrook, S., Roser, S., & Tilch, N. (2004). Hydrological process representation at the meso-scale: The potential of a distributed, conceptual catchment model. *Journal of Hydrology*, *291*(3–4), 278–296. https://doi.org/10.1016/j.jhydrol.2003.12.038

Van Hook, W. A. (1968). Vapor pressures of the isotopic waters and ices. *The Journal of Physical Chemistry*, *72*(4), 1234–1244. https://doi.org/10.1021/j100850a028

Wilcox, D. C. (2008). Formulation of the k-w turbulence model revisited. *AIAA Journal*, *46*(11), 2823–2838. https://doi.org/10.2514/1.36541

Windhorst, D., Kraft, P., Timbe, E., Frede, H.-G., & Breuer, L. (2014). Stable water isotope tracing through hydrological models for disentangling runoff generation processes at the hillslope scale. *Hydrology and Earth System Sciences*, *18*(10), 4113–4127. https://doi.org/10.5194/hess-18-4113-2014

Wong, T., Nusbaumer, J., & Noone, D. (2017). Evaluation of modeled land-atmosphere exchanges with a comprehensive water isotope fractionation scheme in version 4 of the community land model. *Journal of Advances in Modeling Earth Systems*, *9*(2), 978–1001. https://doi.org/10.1002/2016MS000842

Yang, G., Weigand, B., Terzis, A., Weishaupt, K., & Helmig, R. (2018). Numerical simulation of turbulent flow and heat transfer in a three-dimensional channel coupled with flow through porous structures. *Transport in Porous Media*, *122*(1), 145–167. https://doi.org/10.1007/s11242-017-0995-9

Zhou, T., Simunek, J., Braud, I., & Braud, I. (2021). Adapting HYDRUS-1D to simulate the transport of soil water isotopes with evaporation fractionation. *Environmental Modeling & Software*, *143*, 105118. https://doi.org/10.1016/j.envsoft.2021.105118